Research Article

Myoglobin/Gold Nanoparticles/Carbon Spheres 3-D Architecture for the Fabrication of a Novel Biosensor

Xiao Chen, Jing Jing Zhang, Jie Xuan, and Jun Jie Zhu (✉)

Key Laboratory of Analytical Chemistry for Life Science, Ministry of Education, School of Chemistry and Chemical Engineering, Nanjing University, Nanjing 210093, China

ABSTRACT

A novel biosensor based on a myoglobin/gold nanoparticles/carbon spheres (Mb–AuNPs–CNs) 3-D architecture bioconjunction has been fabricated for the determination of hydrogen peroxide (H_2O_2). Cyclic voltammetry (CV), Fourier transform infrared (FT-IR) spectroscopy and scanning electron microscopy (SEM) were used to characterize the bioconjunction of the AuNPs–CNs with Mb. Experimental results demonstrate that the AuNPs–CNs hybrid material is more effective in facilitating electron transfer of the immobilized enzyme than CNs alone, which can be attributed to the unique nanostructure and larger surface area of the bioconjunction. The biosensor displayed good performance for the detection of H_2O_2 with a wide linear range from 0.28 μmol/L to 116.5 μmol/L and a detection limit of 0.12 μmol/L. The Michaelis–Menten constant K_M^{app} value was estimated to be 0.3 mmol/L. The resulting biosensor exhibited fast amperometric response, and good stability, reproducibility, and selectivity to H_2O_2.

Introduction

The design of mediator-free third generation enzyme electrodes, which enable the detection of chemical/biological molecules by a direct electron transfer between the enzyme and the conjoint electrode, is of considerable interest and importance. Extensive work has been carried out with redox protein films over the past few decades in order to find methods to increase the electron transfer rate between enzyme and electrode [1–8]. For example, a variety of carbon-based materials such as carbon nanotubes (CNTs) [9–11] and carbon nanofibers (CNFs) [12, 13] have been successfully employed for the direct electron transfer of proteins in films. Their properties of hydrophilicity, nontoxicity, excellent film-forming ability, and remarkable biocompatibility offer excellent prospects for biocompatible immobilization matrices and the design of novel biosensors. Carbon spheres (CNs), with similar electrochemical properties to CNTs, are spherical structures with a carbonized core and a hydrophilic surface. The complete surface of the carbon spheres can be activated by synthesis using aqueous glucose solutions [14]. Carbon spheres have a large functionalized surface available for loading with noble metal nanoparticles and binding with

Address correspondence to jjzhu@nju.edu.cn

proteins due to the large number of functional groups furnished by the starting materials. Moreover, the cavities in carbon spheres may provide a protective microenvironment for the enzymes, facilitating retention of their stability and activity. In contrast, the use of CNTs in biosensors is limited by the fact that their closed shell does not allow for a high degree of functionalization [9, 15]. Therefore, carbon spheres may be of more interest since they have potential advantages for many advanced applications. To our best knowledge, only a few studies of the use of carbon spheres in electrochemical immunoassay have been reported [16]. Such limited attention is not consistent with the remarkable properties and potential merits of carbon spheres.

Myoglobin (Mb) is a single-chain protein of 153 amino acids containing a heme (iron-containing porphyrin) group in the center which is found in mammalian skeleton and muscle tissues. Mb functions physiologically in the storage of oxygen and in the enhancement of the rate of oxygen diffusion, and has catalytic activity for H_2O_2 decomposition similar to horseradish peroxidase [17, 18]. It is an ideal model molecule for the study of electron transfer reactions of heme proteins and also for biosensing and biocatalysis. However, the direct electron transfer between the redox center of the immobilized enzyme and an electrode is often shielded by the insulating outer protein shell [19]. Because of their controllable size and functional surface, carbon spheres act as meso-scale connectors to bind the enzyme and enhance the possibility of direct electron transfer between protein and electrode surface. Furthermore, a core-shell hybrid material fabricated by coating carbon spheres with citrate-stabilized gold nanoparticles (AuNPs) can optimize the use of carbon spheres in fabricating an immunosensor [16]. Therefore, exploitation of this hybrid material for construction of a Mb-based mediator free H_2O_2 biosensor is a promising area of research.

In the work described here, Mb was immobilized on such a hybrid material to form a myoglobin/gold-nanoparticles/carbon spheres (Mb–AuNPs–CNs) 3-D architecture bioconjunction that can be assembled on a glassy carbon electrode (GCE) for the construction of a novel biosensor. Scanning electron microscopy (SEM) was used to monitor the fabrication process and FT-IR was employed to investigate the conformation. This proposed strategy for the preparation of the hybrid material is simple and effective. The direct electrochemistry and analytical performance of the resulting biosensor in the determination of hydrogen peroxide have been investigated.

1. Experimental

1.1 Reagents

Glucose (analytical purity) was purchased from Beijing Chemical Reagent Factory. Mb (from horse heart) was obtained from Sigma Chemical Co., and used as received. Chloroauric acid ($HAuCl_4 \cdot 4H_2O$), trichloroacetic acid (TCA), trisodium citrate, and hydrogen peroxide (H_2O_2, 30%, w/v solution) were obtained from Shanghai Chemical Reagent Co. Poly(diallyldimethylammonium chloride) (PDDA, 20%, w/w in water, MW = 200,000–350,000) was from Sigma-Aldrich Chemical Co. Nafion, a 5 wt% solution in a mixture of lower aliphatic alcohols and 20% water, was obtained from Aldrich. All chemicals were of analytical grade and used without further purification.

The 0.1 mol/L phosphate buffer solutions (PBS) with different pH values were prepared by mixing stock standard solutions of Na_2HPO_4 and NaH_2PO_4 and adjusting the pH with 0.1 mol/L H_3PO_4 or NaOH. A 0.20% PDDA solution was prepared by diluting 20% PDDA with 20 mmol/L Tris and 20 mmol/L NaCl solution. A 0.5% Nafion solution was prepared by diluting the 5% Nafion solution with ethanol. Electrochemical impedance spectroscopy (EIS) experiments were performed in 0.1 mol/L KCl solution containing 10.0 mmol/L $Fe(CN)_6^{3-}$/$Fe(CN)_6^{4-}$ (1:1). All aqueous solutions were prepared with distilled water.

1.2 Apparatus and measurements

Scanning electron micrographs (SEM) were obtained with a Hitachi S4800 scanning electron microscope. Fourier transform infrared (FT-IR) spectra were

recorded on a Vector 22 FT-IR spectrometer (Bruker). Static water contact angles were measured at 25°C by a contact angle goniometer (Rame-Hart-100) employing drops of pure water. The readings were stabilized and taken within 120 s after addition. Powder X-ray diffraction (XRD) data were collected on a Shimadzu XD-3A X-ray diffractometer (Cu Kα radiation, $\lambda = 0.154\,18$ nm).

Electrochemical measurements were performed on a CHI 630 electrochemical workstation (Chenhua, Shanghai, China) with a conventional three-electrode system comprising a platinum wire as the auxiliary electrode, a saturated calomel electrode (SCE) as the reference and a modified GCE as the working electrode. EIS analyses were performed with an Autolab PGSTAT12 (Eco Chemie BV, The Netherlands) and controlled by GPES 4.9 and FRA 4.9 software with a three-electrode system.

1.3   Preparation of Mb–AuNPs–CNs bioconjuction

The hybrid material AuNPs–CNs were synthesized according to Ref. [16]. CNs were synthesized in aqueous glucose solutions via a microwave-hydrothermal route. The CNs were then dispersed in PDDA solution and stirred for 20 min. After centrifugation and rinsing three times in distilled water, the resulting CNs were then dispersed in a Au colloid solution and stirred for another 20 min.

AuNPs–CNs hybrids (15 mg) or CNs were dispersed in a solution of Mb (2 mg/mL) and stirred for 24 h to allow protein adsorption. The resulting materials were then centrifuged and washed three times with 0.1 mol/L PBS (pH 6.0). By calculating the difference in the concentration of the protein before and after adsorption, we found that about 268 μg of Mb was immobilized onto each mg of AuNPs–CNs hybrid in the the fabrication of the Mb–AuNPs–CNs 3-D architecture bioconjunction.

1.4   Preparation of biosensors based on Mb–AuNPs–CNs and Mb–CNs

A GCE with a diameter of 3 mm was first polished to a mirror surface with a 0.05 μm α-Al$_2$O$_3$ slurry, and then successively ultrasonicated in distilled water and ethanol. The cleaned electrode was dried with a stream of nitrogen immediately before use. 19.1 mg

Mb–AuNPs–CNs bioconjunction or Mb–CNs hybrid material was redispersed in 1 mL of 0.1 mol/L PBS (pH 6.0), and 5 μL of these suspensions were deposited on the surface of a pretreated GCE. They were then left to dry at 4 °C. 0.5% Nafion solution was then added for encapsulation. The electrodes were stored for 24 h at 4 °C when not in use.

2. Results and discussion

2.1   Characterization of the Mb–AuNPs–CNs hybrids

In order to confirm the assembly of AuNPs on the CNs, the materials were investigated by SEM. Figure 1(a) shows that CNs with an average diameter of 250 nm were uniform in size and morphology. Making a comparison between Figs. 1(a) and 1(b), the distinctive difference in morphology before and after loading with AuNPs can be observed. The numerous individual light nanodots shown in Fig. 1(b) are well-dispersed AuNPs which decorate the CNs surface quite uniformly.

Figure 1(c) shows the energy-dispersive (EDS) analysis of the AuNPs–CNs hybrids. The atomic percentages of carbon and gold are 73.4% and 4.0%, respectively. What is also worth noting is that the atomic percentage of oxygen is 18.1%, suggesting the presence of oxygen-containing functional groups from the starting materials.

Figure 1(d) shows the X-ray diffraction pattern of the AuNPs–CNs hybrids. All the diffraction peaks can be indexed to a typical face-centered cubic (fcc) lattice, in good agreement with the standard pattern for metallic Au. The diffraction peaks at $2\theta = 38.3°$, 43.5°, 65.0°, and 77.7° can be assigned to the (111), (200), (220), and (311) reflections of Au.

Contact angle measurements were carried out in order to investigate changes in the properties of the carbon sphere surfaces after immobilization of AuNPs. As shown in Figs. 1(e) and 1(f), the CNs and AuNPs–CNs gave contact angles of 47.5° and 33°, respectively. The hybrid material shows a lower contact angle, indicating a better hydrophilic surface for enzyme adhesion, which should improve the biocompatibility of the electrode surface and facilitate retention of enzyme activity.

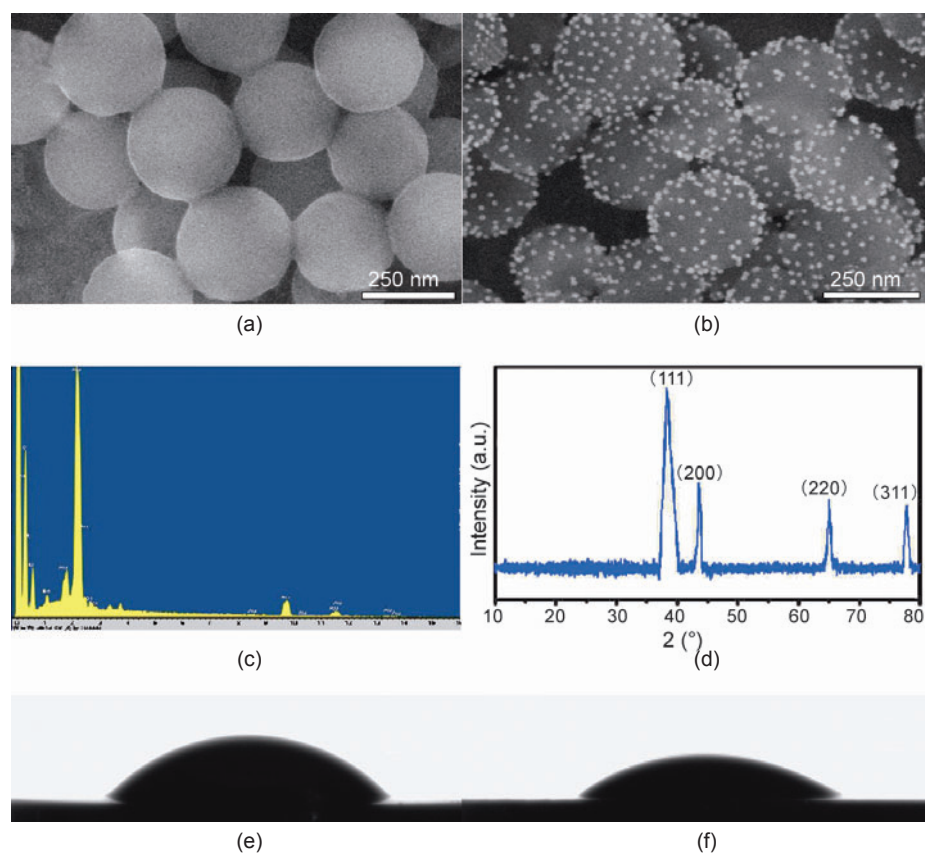Mb entrapped in the composite film was

Figure 1 SEM images of (a) CNs and (b) AuNPs–CNs hybrids; (c) EDS image of AuNP–CNs hybrid material; (d) XRD pattern of AuNP–CNs hybrid material; Contact angles of GCE modified with (e) CNs and (f) AuNPs–CNs hybrids
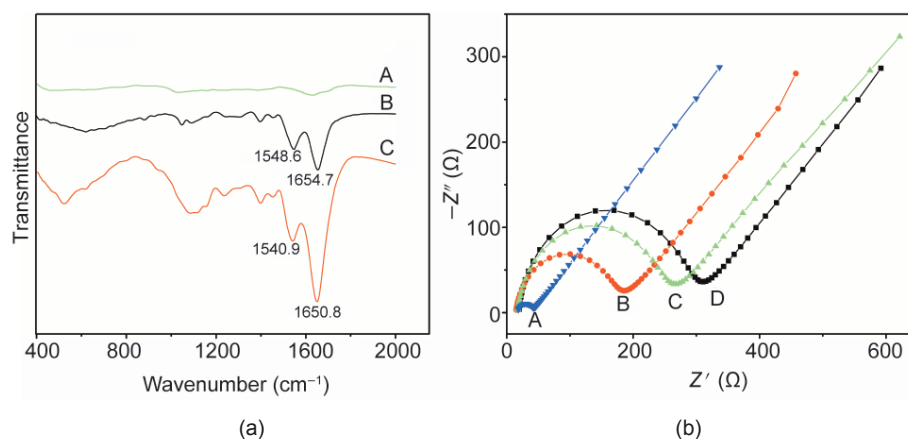

Figure 2 (a) FT-IR spectra of (A) AuNPs–CNs, (B) Mb, and (C) Mb–AuNPs–CNs films; (b) electrochemical impedance spectroscopy for (A) bare GCE, (B) AuNPs–CNs, (C) Mb–AuNPs–CNs, and (D) CNs/GCE recorded in 0.1 mol/L KCl solution containing 10.0 mmol/L $Fe(CN)_6^{3-}/Fe(CN)_6^{4-}$ (1:1)

chains. The amide I band (in the range 1700−1600 cm^{-1}) is ascribed to C=O stretching vibrations of peptide linkages in the protein backbone. The amide II band (in the range 1600−1500 cm^{-1}) is attributed to a combination of N–H in plane bending and C–N stretching of the peptide groups. The spectrum of the AuNPs–CNs precursor (curve A in Fig. 2(a)) shows no obvious spectral features. As shown in plot C in Fig. 2(a), the positions of the amides I (1650.8 cm^{-1}) and II (1540.9 cm^{-1}) bands of Mb in the Mb–AuNPs–CNs hybrid were nearly the same as those (amide I, 1654.7 cm^{-1}; amide II, 1548.6 cm^{-1}) of native Mb (curve B in Fig. 2(a)). This indicates that the essential features of the native Mb secondary structure were mostly retained in Mb–AuNPs–CNs, implying that the porous structure of the hybrid offers a protective microenvironment allowing Mb to retain its enzymatic stability and activity. The slight shifts of amide I bands (from 1654.7 to 1650.8 cm^{-1}) and amide II bands (from 1540.9 to 1548.6 cm^{-1}) suggest some interaction between Mb and the AuNPs–CNs hybrid. The AuNPs–CNs film may provide a promising matrix for Mb immobilization and biosensor fabrication due to its satisfactory biocompatibility.

The fabrication process was also monitored by EIS. The redox couple $Fe(CN)_6^{3-}/Fe(CN)_6^{4-}$ is widely used as an electrochemical probe in electrochemical

investigated by FT-IR spectroscopy, which is an effective method to probe the secondary structure of proteins. The characteristic amide I and amide II bands of proteins provide detailed information about the secondary structure of the polypeptide

impedance studies, especially for the characterization of biomaterial-modified electrodes. Figure 2(b) shows Nyquist plots for bare GCE, AuNPs–CNs/GCE, Mb–AuNPs–CNs/GCE, and CNs/GCE. At a bare GCE, the redox process of the $Fe(CN)_6^{3-}/Fe(CN)_6^{4-}$ probe showed an electron transfer resistance of about 17 Ω (curve A in Fig. 2(b)). When the GCE was modified by carbon spheres (curve D in Fig. 2(b)), the diameter of the semicircle increased to 309 Ω. The AuNPs–CNs hybrid (curve B in Fig. 2(b)) showed far less resistance with the semicircle diameter being 177 Ω, suggesting the hybrid has an excellent electrical conductivity. When Mb was immobilized on the AuNPs–CNs hybrid (curve C in Fig. 2(b)), the electron transfer resistance was slightly increased to 259 Ω. Owing to the dielectric behavior of enzyme molecules for interfacial electron transfer processes, the higher enzyme coverage will result in a higher barrier for interfacial electron transfer. These data confirm that Mb had been successfully immobilized on the AuNPs–CNs hybrid and blocked the electron exchange between the redox probe and the electrode.

2.2 Direct electron transfer of the biosensor

Figure 3(a) shows typical cyclic voltammograms (CVs) for CNs/GCE, Mb–CNs/GCE, AuNPs–CNs/GCE, and Mb–AuNPs–CNs/GCE at a scan rate of 0.2 V/s. No obvious redox peaks were observed at the CNs/GCE (curve A) and AuNPs–CNs/GCE (curve C), which suggests that neither CNs nor AuNPs–CNs were electroactive in the potential range studied. The CV of Mb–CNs/GCE (curve B) had a pair of quasi-reversible redox peaks, implying direct electron transfer between the immobilized Mb and the electrode. In comparison, the redox peaks observed on the Mb–AuNPs–CNs/GCE (curve D) were remarkably large. The cathodic and anodic peak potentials were −0.399 V and −0.338 V, respectively. The formal potential (E_p), calculated from the average value of cathodic and anodic peak potentials, was −0.369 V, which is characteristic of the reversible electrode process of the heme Fe(III)/Fe(II) redox couple in immobilized Mb. The potential difference between cathodic and anodic peak potentials of 61 mV at this scan rate implies a high speed of the

electron transfer process for the electroactive center of the immobilized Mb. Therefore, it can be concluded that direct electron transfer between the Mb and electrode is greatly enhanced by the presence of the AuNPs–CNs hybrids which provide a biocompatible microenvironment for the entrapped Mb.

Figure 3(b) displays the CVs of Mb–AuNPs–CNs/GCE with varying scan rates from 0.05 to 0.5 V/s. The cathodic and anodic peak currents of Mb both increased with increasing scan rates, and the cathodic and anodic peak potentials showed a slight shift and the peak to peak separation also increased. As shown in the inset of Fig. 3(b), both the cathodic and anodic peak currents increased linearly with scan rates from 0.05 to 0.5 V/s. This indicates that the electron transfer between Mb and GCE is not difficult and that it is a surface-controlled electrochemical process. According to the Laviron method for a surface-controlled electrochemical system [20], the apparent heterogeneous electron transfer rate constant (k_s) of Mb immobilized on Mb–AuNPs–CNs/GCE was estimated to be about 6.7 s^{-1}. This value of k_s is higher than those reported for systems involving Mb or hemoglobin (Hb) immobilized on various inorganic hybrid films without metal nanoparticles, such as a Mb/multi-walled carbon nanotube film (5.4 s^{-1}) or an Hb–Nafion–CNF/GCE (2.4 s^{-1}) [3, 13], suggesting that the presence of the AuNPs enhanced the electron transfer rate of Mb immobilized on the AuNPs–CNs hybrid. According to Faraday's law, $Q = nFA\Gamma^*$, where F is Faraday constant. The charge Q can be obtained by integrating the reduction peak of Mb, and n and A stand for the number of electrons transferred and the geometrical surface area of the electrode (3 mm diameter), respectively. From this equation, the surface concentration of electroactive Mb (Γ^*) at Mb–AuNPs–CNs/GCE was estimated to be 1.61×10^{-10} mol/cm^2. This value is an order of magnitude higher than that of the theoretical monolayer coverage (1.58×10^{-11} mol/cm^2) estimated on the basis of the crystallographic dimensions of 3.0 nm × 3.5 nm × 2.3 nm for Mb [21], assuming each molecule has its long axis parallel to the electrode surface. This suggests that the matrix may trap multiple layers of Mb and greatly facilitate approach of its active site to the electrode.
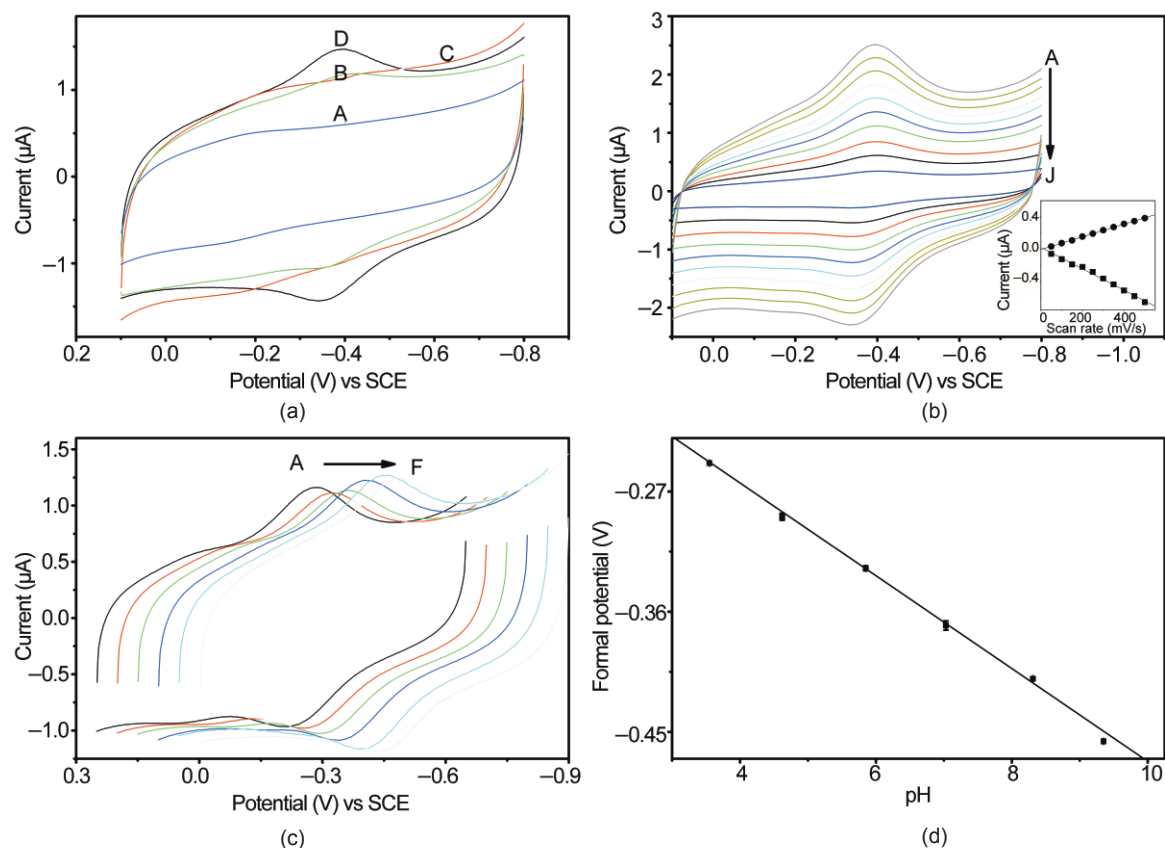
Figure 3 (a) Cyclic voltammograms of (A) CNs/GCE, (B) Mb–CNs/GCE, (C) AuNPs–CNs/GCE, and (D) Mb–AuNPs–CNs/GCE in 0.1 mol/L pH 7.0 PBS at a scan rate of 0.2 V/s; (b) cyclic voltammograms of Mb–AuNPs–CNs/GCE in 0.1 mol/L PBS (pH 7.0) with different scan rates (V/s): (A) 0.5, (B) 0.45, (C) 0.4, (D) 0.35, (E) 0.3, (F) 0.25, (G) 0.2, (H) 0.15, (I) 0.1, (J) 0.05, and (Inset) plot of peak currents vs. scan rates; (c) cyclic voltammograms of Mb–AuNPs–CNs/GCE in 0.1 mol/L PBS (pH 7.0) with different pH: (A) 3.55, (B) 4.62, (C) 5.85, (D) 7.03, (E) 8.31, (F) 9.35 at a scan rate of 0.2 V/s; (d) plot of formal potential vs pH in 0.1 mol/L PBS at a scan rate of 0.2 V/s
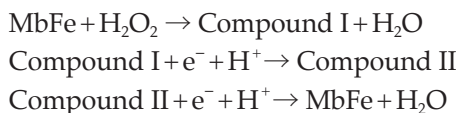
The dependence of the electrochemical behavior of Mb–AuNPs–CNs/GCE on the pH was studied. As shown in Fig. 3(c), the potentials of both reduction and oxidation peaks shifted with the increase of solution pH from 3.55 to 9.35. The pH increase led to a linear negative shift in peak potential (Fig. 3(d)). It is well known that a pH increase can decrease the formal potentials of heme proteins that undergo proton-coupled electron transfer [22]. This redox Bohr effect, a shift in the formal potential as a function of pH, results from the change in the protonation of a water molecule at the sixth coordination position in the heme iron and also protonation of the protolytic groups around the heme with changing pH [23]. The shift in peak potentials for Mb–AuNPs–CNs/GCE with pH therefore indicates that the redox reaction is accompanied by the transfer of protons. The value of the slope (35 mV/pH) was smaller than the theoretically expected value, 59 mV/pH, for a one-electron one-proton reaction [24]. This may be attributed to the influence of the protonation states of the ligands coordinated to the heme iron and the amino acids around the heme, or to the protonation of the water molecule coordinated to the central iron [25].

2.3 Electrocatalytic activity of the biosensor

The determination of H_2O_2 is of great importance in many fields, such as clinical, food, pharmaceutical, and environmental analyses. Figures 4(a) and 4(c) show the bioelectrocatalytic activity of Mb–AuNPs–CNs/GCE and Mb–CNs/GCE for H_2O_2. In the presence of H_2O_2, an obvious increase in the cathodic peak current at around –0.36 V was observed, together with a decrease of anodic peak current. This demonstrates that the electrocatalytic

reduction processes in Mb–AuNPs–CNs/GCE and Mb–CNs/GCE are typical of Mb. A possible mechanism for electrocatalytic reduction of H_2O_2 at an Mb-based enzyme electrode has been reported [26], which can be expressed as follows:

$$MbFe + H_2O_2 \rightarrow \text{Compound I} + H_2O$$
$$\text{Compound I} + e^- + H^+ \rightarrow \text{Compound II}$$
$$\text{Compound II} + e^- + H^+ \rightarrow MbFe + H_2O$$

A significantly stronger peak current was observed for the CV curve for Mb–AuNPs–CNs compared to that for Mb–CNs/GCE as shown in Fig. 4(d). Such enhanced Faradic responses are of great importance in voltammetric investigations of interfacial electron transfer in redox proteins, and are also highly desired for development of new biosensors. The observed currents for the Mb–AuNPs–CNs/GCE and Mb–CNs/GCE electrodes both showed a good linear relationship with the concentration of H_2O_2 in the range 0.28–116.5 μmol/L and 14.2–72.5 μmol/L, respectively. The linear regression equations for Mb–AuNPs–CNs/GCE and Mb–CNs/GCE were $I = 0.1189 + 0.03788C$ ($R = 0.999$, $n = 18$) and $I = 0.4704 + 0.02528C$ ($R = 0.995$, $n = 8$) respectively. From the slope of 0.03788 μA/(μmol/L), the limit of detection for Mb–AuNPs–CNs/GCE was estimated to be 0.12 μmol/L at a signal-to-noise ratio of 3σ. Mb–AuNPs–CNs/GCE showed a significantly better electrocatalytic response to H_2O_2 than Mb–CNs/GCE, which can possibly be attributed to the unique electronic properties of AuNPs on account of their quantum size confinement and biocompatability.

When the concentration of H_2O_2 was higher than 116.5 μmol/L, a response plateau was observed, showing the characteristics of the Michaelis–
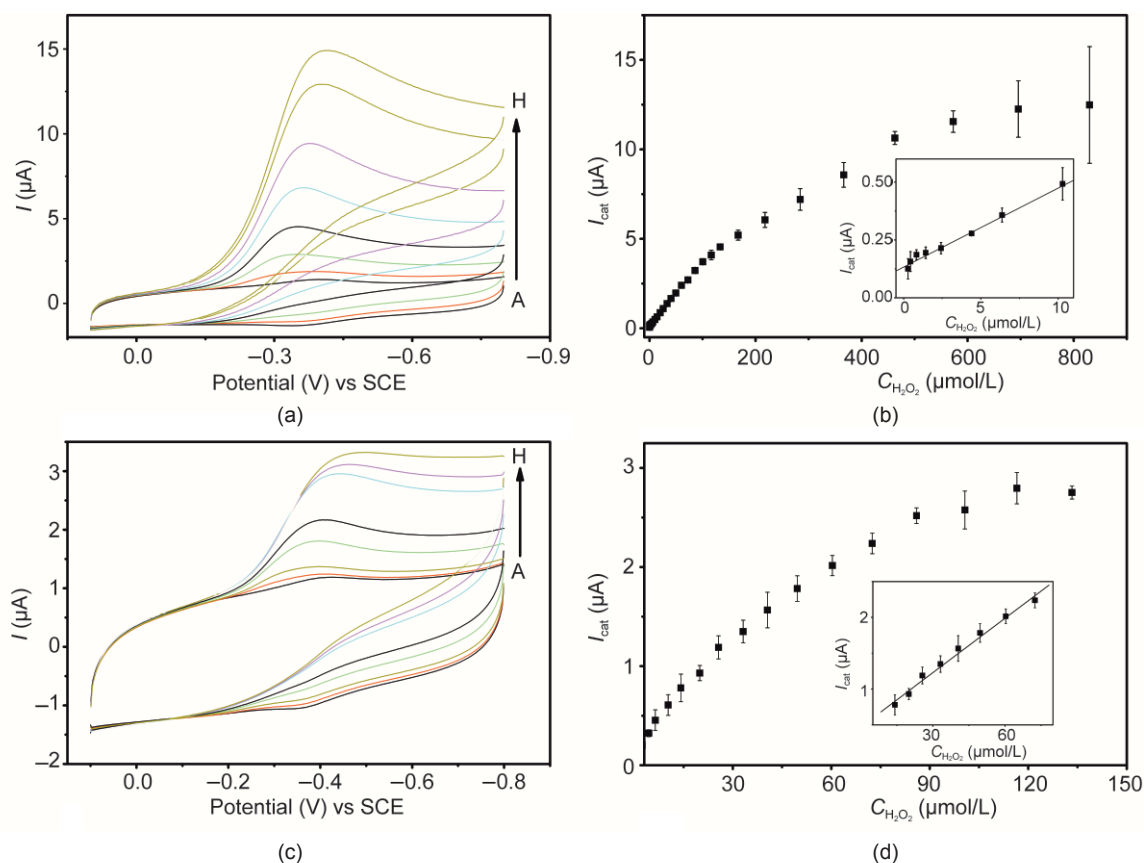

Figure 4   (a) Cyclic voltammograms of Mb–AuNPs–CNs/GCE in 0.1 mol/L PBS (pH 7.0) with H_2O_2 concentrations (μmol/L) of (A) 0, (B) 14.2, (C) 40.6, (D) 86.0, (E) 167.3, (F) 284.3, (G) 462.7, and (H) 572.8 (scan rate, 0.2 V/s); (b) plots of electrocatalytic current (I_{cat}) vs H_2O_2 concentration for Mb–AuNPs–CN/GCE and (Inset) linear plots of I_{cat} vs H_2O_2 concentration; (c) cyclic voltammograms of Mb–CNs/GCE in 0.1 mol/L PBS (pH 7.0) with H_2O_2 concentrations (μmol/L) of (A) 0, (B) 0.04, (C) 0.836, (D) 10.3, (E) 20.0, (F) 40.6, (G) 49.6, and (H) 60.3 (scan rate, 0.2 V/s); (d) plots of electrocatalytic current (I_{cat}) vs H_2O_2 concentration for Mb–CNs/GCE and (Inset) linear plots of I_{cat} vs H_2O_2 concentration

Menten kinetic mechanism. The apparent Michaelis–Menten constant (K_M^{app}), which gives an indication of the enzyme-substrate kinetics, can be obtained from the electrochemical version of the Lineweaver–Burk equation [27]:

$$\frac{1}{I_{ss}} = \frac{1}{I_{max}} + \frac{K_M^{app}}{I_{max}C}$$

where I_{ss} is the steady-state current after the addition of substrate, which can be obtained from CV, I_{max} is the maximum current under saturated substrate conditions and C is the bulk concentration of the substrate. The value of the apparent Michaelis–Menten constant (K_M^{app}) can be determined by the slope (K_M^{app}/I_{max}) and the intercept ($1/I_{max}$) for the plot of the reciprocal of the steady-state current (I_{ss}) versus the reciprocal of H_2O_2 concentration (C). This plot had a good linear relationship, since the linear regression equation was $1/I_{ss} = 0.0694 + 20.8/C$ ($R = 0.999$, $n = 19$). Accordingly, the K_M^{app} value for the Mb–AuNPs–CNs/GCE was estimated to be 0.30 mmol/L. This value is smaller than the reported values of 0.68 mmol/L for Hb–CNT powder microelectrodes [28] and 1.22 mmol/L for clay–Mb–AuCS–GCE [29], implying that our modified electrode exhibited a higher affinity for H_2O_2.

It was also found that Mb–AuNPs–CNs/GCE showed bioelectrocatalytic activity for TCA. The detection of TCA is of great importance in pollution control, since it is a common organohalide environmental pollutant. In the presence of TCA a significant increase in the cathodic peak current at around −0.36 V was observed, which suggested that the biosensor also has potential use in detecting such organohalide pollutants in the environment.

2.4 Reproducibility and stability of the hydrogen peroxide biosensor

To evaluate the electrode-to-electrode reproducibility, six Mb–AuNPs–CNs/GCEs were prepared independently under the same conditions. The relative standard deviation (R.S.D.) of the prepared biosensors was 4.4%. The R.S.D. for six successive determinations at an H_2O_2 concentration of 4 μmol/L was 1.9%. These results are better than the corresponding values for Mb in a ZrO_2-grafted collagen hybrid [30], which

were 5.5% for electrode–electrode reproducibility and 3.2% for successive determinations on one electrode, indicating the excellent reproducibility of Mb–AuNPs–CNs/GCE.

The storage stability of the Mb–AuNPs–CNs/GCE was also studied. When not in use, the electrode was kept at 4 °C in a refrigerator. The response to 40 μmol/L H_2O_2 retained 93.6% of its initial current after 30 days storage. This good long-term stability can be attributed to the good biocompatibility of the composite, which can provide a favorable microenvironment for retention of the bioactivity of Mb.

2.5 Selectivity of the hydrogen peroxide biosensor

The selectivity of the new H_2O_2 biosensor was evaluated by studying the effect of adding substances that might interfere with the determination of H_2O_2. The results are shown in Table 1. When concentrations of glucose, glycine, ascorbic acid, citric acid, ethanol, and acetic acid coexisting in the sample were twice that of H_2O_2, no significant interference was observed, indicating that these species did not affect the determination of H_2O_2. The high selectivity of the Mb–AuNPs–CNs/GCE biosensor verified its applicability for real sample analysis.

3. Conclusions

In this work, carbon spheres were combined with gold nanoparticles and Mb to form a myoglobin/gold nanoparticles/carbon spheres (Mb–AuNPs–CNs) 3-D architecture bioconjunction, which can be used to construct a mediator-free H_2O_2 biosensor. The biosensor was more effective in facilitating the electron transfer of immobilized enzyme than using CNs alone, which can be attributed to the unique nanostructure and large surface area of the bioconjunction. The biosensor displayed broader linear range and lower detection limit for H_2O_2 determination, as compared to CNs-based H_2O_2 biosensors. Furthermore, the good long-term stability and reproducibility of this biosensor demonstrate its applicability for practical biomedical detection and environmental analysis.

Table 1 Interference of various substrates (20 μmol/L) on the response of the Mb–AuNPs–CNs/GCE to 10 μmol/L H_2O_2 in 0.1 mol/L PBS (pH = 7.0)

Substrate	Current ratio	Relative standard deviation (n=6) (%)
Glucose	1.03 ± 0.12	4.7
Hlycine	1.02 ± 0.13	5.4
Ascorbic acid	0.93 ± 0.096	3.9
Citric acid	0.957 ± 0.073	3.0
Ethanol	1.002 ± 0.03	1.3
Acetic acid	0.939 ± 0.09	3.7

Acknowledgements

References

[1] Rusling, J. F.; Nassar, A. E. F. Enhanced electron-transfer for myglobin in surfactant films on electrodes. *J. Am. Chem. Soc.* **1993**, *115*, 11891–11897.

[2] Nassar, A. E. F.; Bobbitt, J. M.; Stuart, J. D.; Rusling, J. F. Catalytic reduction of organohalide pollutants by myoglobin in a biomembrane-like surfactant film. *J. Am. Chem. Soc.* **1995**, *117*, 10986–10993.

[3] Zhao, G. C.; Zhang, L.; Wei, X. W.; Yang, Z. S. Myoglobin on multi-walled carbon nanotubes modified electrode: Direct electrochemistry and electrocatalysis. *Electrochem. Commun.* **2003**, *5*, 825–829.

[4] Cai, C. X.; Chen, J. Direct electron transfer and bioelectrocatalysis of hemoglobin at a carbon nanotube electrode. *Anal. Biochem.* **2004**, *325*, 285–292.

[5] Zhou, H. H.; Chen, H.; Luo, S. L.; Chen, J. H.; Wei, W. Z.; Kuang, Y. F. Glucose biosensor based on platinum microparticles dispersed in nano-fibrous polyaniline. *Biosens. Bioelectron.* **2005**, *20*, 1305–1311.

[6] Zhang, L.; Jiang, X.; Niu, L.; Dong, S. J. Syntheses of fully sulfonated polyaniline nano-networks and its application to the direct electrochemistry of cytochrome *c. Biosens. Bioelectron.* **2006**, *21*, 1107–1115.

[7] Zhang, L.; Zhang, Q.; Li, J. H. Direct electrochemistry and electrocatalysis of hemoglobin immobilized in bimodal mesoporous silica and chitosan inorganic–organic hybrid film. *Electrochem. Commun.* **2007**, *9*, 1530–1535.

[8] Liu, X. Q.; Shi, L. H.; Niu, W. X.; Li, H. J.; Xu, G. B. Amperometric glucose biosensor based on single-walled carbon nanohorns. *Biosens. Bioelectron.* **2008**, *23*, 1887–1890.

[9] Sotiropoulou, S.; Chaniotakis, N. A. Carbon nanotube array-based biosensor. *Anal. Bioanal. Chem.* **2003**, *375*, 103–105.

[10] Banks, C. E.; Compton, R. G. Exploring the electrocatalytic sites of carbon nanotubes for NADH detection: An edge plane pyrolytic graphite electrode study. *Analyst* **2005**, *130*, 1232–1239.

[11] Wang, J. Stripping analysis at bismuth electrodes: A review. *Electroanalysis* **2005**, *17*, 1341–1346.

[12] Vamvakaki, V.; Tsagaraki, K.; Chaniotakis, N. Carbon nanofiber-based glucose biosensor. *Anal. Chem.* **2006**, *78*, 5538–5542.

[13] Lu, X. B.; Zhou, J. H.; Lu, W.; Liu, Q.; Li, J. H. Carbon nanofiber-based composites for the construction of mediator free biosensors. *Biosens. Bioelectron.* **2008**, *23*, 1236–1243.

[14] Sun, X. M.; Li, Y. D. Colloidal carbon spheres and their core/shell structures with noble–metal nanoparticles. *Angew. Chem.* **2004**, *116*, 607–611.

[15] Balasubramanian, K.; Burghard, M. Electrochemically functionalized carbon nanotubes for device applications. *Small* **2005**, *1*, 180–192.

[16] Cui, R. J.; Liu, C.; Shen, J. M.; Gao, D.; Zhu, J. J.; Chen, H. Y. Gold nanoparticle–colloidal carbon nanosphere hybrid material: Preparation, characterization, and application

for an amplified electrochemical immunoassay. *Adv. Funct. Mater*. **2008**, *18*, 2197–2204.

[17] Stargardt, J. F.; Hawkridge, F. M.; Landrum, H. L. Reversible heterogenous reduction and oxidation of sperm whale myoglobin at a surface modified gold minigrid electrode. *Anal. Chem*. **1978**, *50*, 930–932.

[18] Hildebrand, D. P.; Tang, H. L.; Luo, Y. G.; Hunter, C. L.; Smith, M.; Brayer, G. D.; Mauk, A. G. Efficient coupled oxidation of heme by an active site variant of horse heart myoglobin. *J. Am. Chem. Soc*. **1996**, *118*, 12909–12915.

[19] Yabuki, S.; Shinohara, H.; Aizawa, M. Electro-conductive enzyme membrane. *J. Chem. Soc. Chem. Commun*. **1989**, 945–946.

[20] Laviron, E. General expression of the linear potential sweep voltammogram in the case of diffusionless electrochemical systems. *J. Electroanal. Chem*. **1979**, *101*, 19–28.

[21] Kendrew, J. C.; Bodo, G.; Dintzis, H. M.; Parrish, R. G.; Wyckoff, H.; Phillips, D. C. A three-dimensional model of the myoglobin molecule obtained by X-ray analysis. *Nature* **1958**, *181*, 622–666.

[22] Leitch, F. A.; Moore, G. R.; Pettigrew, G. W. Structural basis for the variation of pH-dependent redox potentials of Pseudomonas cytochromes *C*-551. *Biochem*. **1984**, *23*, 1831–1838.

[23] Wyman, J. Regulation in macromolecules, as illustrated by hemoglobin. *Quart. Rev. Biophys*. **1968**, 35–80.

[24] Bond, A. M. *Modern Polarographic Methods in Analytical Chemistry*. M. Dekker: New York, 1980, pp. 27–45.

[25] Yamazaki, I.; Araiso, T.; Hayashi, Y.; Yamada, H.; Makino, R. Analysis of acid-base properties of peroxidase and myoglobin. *Adv. Biophys*. **1978**, *11*, 249–281.

[26] Tatsuma, T.; Mori, H.; Fujishima, A. Electron transfer from diamond electrodes to heme peptide and peroxidase. *Anal. Chem*. **2000**, *72*, 2919–2924.

[27] Kamin, R. A.; Wilson, G. S. Rotating-ring-disk enzyme electrode for biocatalysis kinetic-studies and characterization of the immobilized enzyme layer. *Anal. Chem*. **1980**, *52*, 1198–1205.

[28] Zhao, Y. D.; Bi, Y. H.; Zhang, W. D.; Luo, Q. M. The interface behavior of hemoglobin at carbon nanotube and the detection for H_2O_2. *Talanta* **2005**, *65*, 489–494.

[29] Zhao, X. J.; Mai, Z. B.; Kang, X. H.; Dai, Z.; Zou, X.Y. Clay–chitosan–gold nanoparticle nanohybrid: Preparation and application for assembly and direct electrochemistry of myoglobin. *Electrochim. Acta* **2008**, *53*, 4732–4739.

[30] Zong, S. Z.; Cao, Y.; Zhou, Y. M.; Ju, H. X. Reagentless biosensor for hydrogen peroxide based on immobilization of protein in zirconia nanoparticles enhanced grafted collagen matrix. *Biosens. Bioelectron*. **2007**, *22*, 1776–1782.